JOURNAL OF MATERIALS SCIENCE 17 (1982) 477–498

Composites of aluminium alloys: fabrication and wear behaviour

F. M. HOSKING*, F. FOLGAR PORTILLO, R. WUNDERLIN†, R. MEHRABIAN‡
Department of Metallurgy and Mining Engineering, University of Illinois, Urbana, Illinois 61801, USA

In this paper processes for fabrication of aluminium-alloy composites containing particulate non-metals, the net shape forming of these composites, their microstructures, their friction and wear behaviours and their mechanical properties are described. Composites of two wrought (2014 and 2024) and one cast (201) aluminium alloys containing 2 to 30 wt% of Al_2O_3 and SiC particles in the size range of 1 to 142 μm were prepared. The non-metallic particles were added to a partially-solid vigorously-agitated matrix alloy. The particles were then retained in the matrix until interface interaction, for example, the formation of $MgAl_2O_4$ spinel in the case of Al_2O_3 particles, were faciliated. These composites were solidified and subsequently reheated to above their liquidus temperature and formed under high pressure in a closed-die forging type of apparatus. Composites with particulate additions of size larger than 5 μm possessed homogeneous structures; particles of size 1 μm, however, tended to cluster. The wear behaviour of the composites was studied using a pin-on-disc type machine. It was shown that composites containing large amounts of non-metals, ~ 20 wt%, exhibit excellent wear resistance whilst those with small to moderate amounts of non-metals possess tensile properties comparable to the matrix alloy. Increasing the amount of particulate additions results in reduced ductility. Finally, a method was investigated of producing components with high weight-fractions of non-metals near their surface.

1. Introduction

Much work has been stimulated starting from the increased demand for lightweight, energy efficent materials and it is anticipated that inexpensive light metal-matrix composites may find special applications if capable of meeting specific friction and wear requirements while maintaining reasonable mechanical properties. The investigation reported here was aimed at developing wear-resistant composites of aluminium-base alloys by combining them with hard particulate materials. The various composites fabricated were formed into net shapes, and their microstructures, friction and wear behaviour and mechanical properties were studied.

The survey given in this section is divided into two general areas. First, available methods for the preparation of a variety of metal-matrix composites are reviewed and the microstructures produced are related to the mechanical properties. Second, a general description is given of our current understanding of the wear behaviour of alloys containing particulate additions.

1.1. Preparation and mechanical behaviour of metal-matrix composites

A significant portion of the work done in the metal-matrix composites field deals with discontinuous second-phase particles that are uniformly

*Present address: Sandia Laboratories, Albuquerque, New Mexico, USA.
†Present address: FWA, Altenrhein, Switzerland.
‡Present address: Metallurgy Division, National Bureau of Standards, Department of Commerce, Washington DC, USA.

0022–2461/82/020477–22$4.20/0

distributed in an alloy matrix. Oxides, carbides, silicides, borides and other non-metallic dispersoid systems have shown some degree of promise in wear and strengthening.

There are a number of techniques available for the producing of various dispersed-phase alloys. They include solid-state transformations, liquid-liquid reactions, liquid-solid reactions, gas-liquid reactions, gas-solid reactions and mechanical mixing of powders. A promising new technique [1,2] for the production metal-matrix composites containing non-metallic particulates involves taking advantage of the rheological behaviour and structure of a partially-solidified agitated matrix alloy. A limitation of this method includes the difficulty of adding very fine particle sizes without clustering or segregation either prior to addition or within the metal matrix. For moderate size particles (3 to 150 μm), however, the technique permits the fabrication of materials that exhibit improved friction and wear behaviour while maintaining reasonable engineering strength [2]. An important factor leading to the developement of such composites, in addition to improved friction and wear properties, is the consideration of material selection against product economics. It may become practical to replace a more expensive material by a less expensive alloy containing a dispersiod that maintains the same mechanical design requirements.

Studies to evaluate the properties and behaviour of dispersed-phase alloys can be divided into several groups. Of interest to this study is the addition of those particles with sizes greater than 1 μm. The investigation of Edelson and Baldwin [3] on dispersion-strengthened copper alloys considered the behaviour of dispersions of particles larger than one micrometre in size. Powder metallurgy techniques were used to fabricate alloys consisting of dispersions of chromium, iron, alumina, molybdenum, graphite, lead and voids in copper. Particles ranging in size from 5 to 200 μm, volume fractions, g, of 0 to 0.25, mean free-paths, λ, of 25 to 45 μm, and inter-particle spacings, D_s, of 5 to 8 μm were tested, see Fig. 1.

It was shown that iron and chromium particles increased the yield strength. The voids, alumina, graphite, lead and molybdenum dispersions showed no improvemtent. In all cases, strengthening occured when a strong particle–matrix bond was formed and the yield stress was shown to be a function of the mean free-path (that is, particle-size and volume-fraction). The degree of hardening

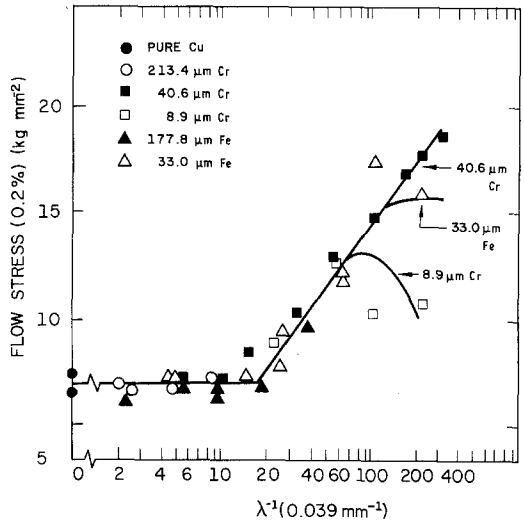

Figure 1 The relation of yield stress to log reciprocal mean free-path between particles in copper–chromium and copper–iron alloys (Gensamer plot), taken from [3].

seemed to fall off above a critical mean free-path whose value varied directly with the particle diameter, as shown in Fig. 1 [3].

Ductility, as measured by reduction in area, is a function of volume-fraction and is independent of particle size. The general trend as shown in a plot of ductility against volume-fraction in Fig. 2 [3], shows the effect of second-phase additions as always being embrittling, regardless of their effects on strengthening. The second phases, especially those with irregular shapes, act as areas where crack

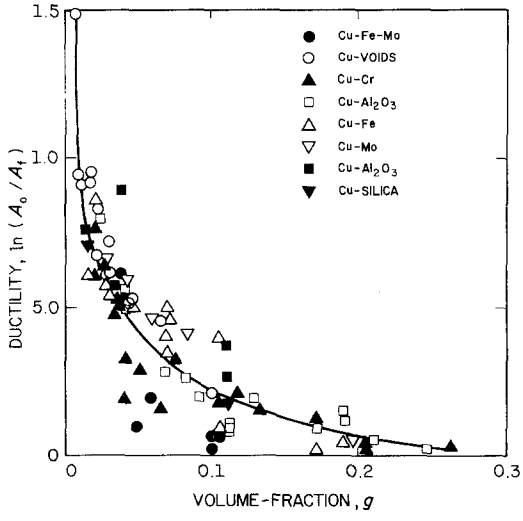

Figure 2 Combined plot of ductility of several copper dispersion alloys against volume-fraction, taken from [3].

initiation and propogation may occur as a result of local stress concentrations.

In two recent studies [4, 5], the interface interactions of alumina fibres (3 to 6 mm long) with aluminium alloys were examined. Composites of homogeneous dispersions of Al_2O_3 fibres were obtained by adding them both to agitated partially-solid slurries and to completely liquid aluminium alloys. In both processes, the fibres appeared wetted and bonded to the matrix. Microscopic examination of the composites revealed the existence of an altered microstructure around the Al_2O_3 fibres which consisted of a fine multi-phase material. Features commmon to all the structures were the existence of an intimate bond, the absence of voids at the fibre boundary and the presence of fine polycrystalline α-Al_2O_3 in the interaction zone. In the case of Al–Mg alloys, bonding was achieved through formation of a $MgAl_2O_4$ (spinel) layer by reaction between the fibre and the Mg in the liquid-Al. The Al–Cu–Mg alloys were observed to have $MgAl_2O_4$, α-Al_2O_3 and possibly $CuAl_2O_4$ co-existing in the interaction zone.

It was postulated [5] that a compound of the aluminate-type that formed on the fibre surface provided the necessary bond with the surrounding matrix which led to strengthening. Examination of fracture surfaces of the composite revealed that, in general, the failure occured, not at the interface, but rather by plastic flow at the matrix around the fibres.

In summary, the properties of coarse particle dispersions seem to be dependent on the geometric variables of dispersion (e.g., the mean free-path, λ) and the structural characteristics of the dispersoid (e.g., strength and bond formation).

1.2. Wear behaviour

Wear is generally defined as the unwanted removal of material by chemical or mechanical action. Wear classifications can depend on such parameters as the wear-rate, the wear mechanism and the type of relative motion. For example, the amount of material lost could be used to define mild or severe wear.

Wear-rate under dry-sliding conditions, which is the subject of this investigation, increases with increasing applied normal load. However, changes in the microsctructure and the microchemistry of an alloy can affect this finding. For example, Bhansali [6] reports that the presence of oxides in nickel-base alloys and carbides in cobalt-base alloys result in anamalous behaviour in the wear-rate as a function of applied load. The effect of sliding velocity on wear-rate is not well defined because it can influence the operating wear mechanism itself.

The mild to severe transition in dry-sliding wear has been the subject of a number of studies [7–9]. It is generally agreed that increasing the hardness of the contact surface pushes this transition to higher loads. For example, Arnell *et al.* [8] report that the mild–severe wear transiton occurs when the maximum shear stress in the region of contact reaches one-sixth of the material hardness. While this simple correlation was deduced from a number of experiments on copper, brass and mild steel against a hardened steel disc, it is unlikely that it would hold for other materials and test conditions.

The presence of discrete hard or soft particles in a matrix can influence wear behaviour in important ways. Both Hogmark *et al.* [10] and Sato *et al.* [2] found reduced wear when the matrix alloy contained hard particles. The presence of soft particles could increase wear rate [2, 11]. However, this observation may have been due to the poor bonding between the particles and the matrix [11].

In general, aluminium alloys display two basic wear mechanisms: oxidative or mild wear and metallic or severe wear. The onset of severe wear is taken as the start of seizure and the sliding distance that corresponds to this point is designated as the "point of seizure". Most studies of dry-sliding wear have been concerned with the effects of applied load, sliding velocity and alloy composition on seizure resistance. For example, it has been found that additions of copper to aluminium improve the seizure resistance, particularly at higher sliding velocities [12]. On the other hand, applied load and, to a lesser extent, sliding velocity influence the point at which seizure occurs, but have no effect on the mechanism of seizure.

Additions of silicon, especially in the hypereutectic composition range, which results in the formation of primary hard silicon particles in the matrix, improves the wear resistance of aluminium alloys. Shivanath *et al.* [13] have shown a continuous increase in the transition load with increasing silicon content in this composition range. However, oxidative wear rates (mild wear) appear to be independent of both silicon content and the particle size of the silicon.

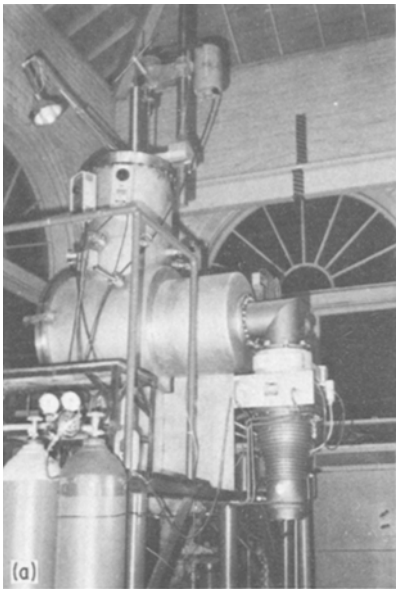

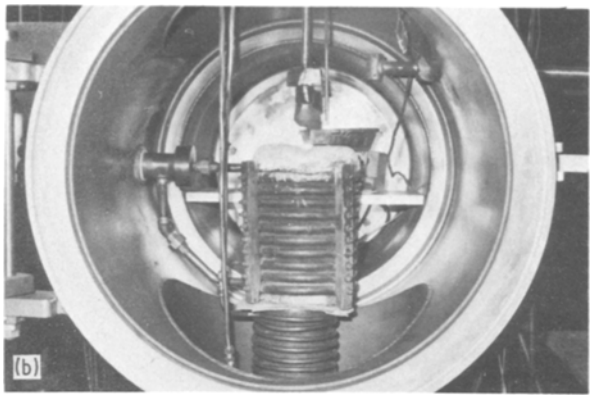

Figure 3 Photographs of the compositing apparatus. (a) shows an overall view of the vacuum system on its stand with its associated pumps, mixing motor, etc. (b) and (c) show close-ups of the chamber, the induction coil, mixing blade and particle addition trough.

2. Apparatus and procedure

Aluminium-matrix composites of two-wrought alloys, Alloy 2014 and Alloy 2024*, and one cast alloy, Alloy 201†, containing particulate additions of Al_2O_3 and SiC were produced in a vacuum-induction melting and casting system especially modified for this purpose. The composite fabrication technique is based on that previously described [2]. The composites were subsequently reheated to above their liquidus temperatures in a second induction furnace and forged into shape in a 200 ton hydraulic press. The microstructures of the composites were studied and their tensile properties were determined. Finally, disc-shaped wear-test specimens were removed from the forged composites and their wear behaviour was studied on a pin-on-disc-type machine designed and constructed for use in this investigation.

2.1. Fabrication of the composites

Photographs and a schematic illustration of the modified vacuum-induction system used to fabricate the composites are shown in Figs 3 and 4. The apparatus consists of an induction power supply (50 kW, 3000 Hz) a water-cooled vacuum chamber with its associated mechanical and diffusion pumps, and a crucible and mixing assembly for agitation of the composites. The composite fabrication included partial solidification of an aluminium melt in vacuum while it was subjected to vigorous agitation. The non-metallic particles were then added to the partially-solid alloy slurry while agitation was continued. The non-metals were thus entrapped in the melt while interaction between the particles and the matrix promoted wetting [1, 2, 5].

The vacuum induction furnace shown in Figs 3 and 4 has several ports for observation of the melt and the incorporation of water, gas and electrical feedthroughs. The mixing assembly located on top of the furnace is co-axially aligned through an O-ring seal at the top of the chamber and a bearing block just above the crucible.

The blades, made of cast iron, were sand-cast and ground with a curved taper. The overall blade dimensions are 76 mm in length, ~ 40 mm in height and ~ 40 mm in width at the centre with a taper down to 6 mm at the blade-tip. Two blades were utilized mounting one perpendicular to the other on the shaft. A protective refractory coating‡ was applied to the blades to prevent interaction with the molten melt. This was further coated with a carbon wash. A conical graphite plug (~ 40 mm in diameter by ~ 40 mm in length) was screwed on

*Alloy 2014 was of nominal composition 4.4 wt% Cu, 0.8 wt% Si, 0.8 wt% Mn, 0.4 wt% Mg, Balance Al. Alloy 2024 was of nominal composition 4.5 wt% Cu, 1.5 wt% Mg, 0.6 wt% Mn, Balance Al.
†Alloy 201 was of nominal composition 4.7 wt % Cu, 0.39 wt % Mg, 0.3 wt % Mn, 0.6 wt % Ag, 0.2 wt % Ti, Balance Al.
‡Sauereisen paste number 1.

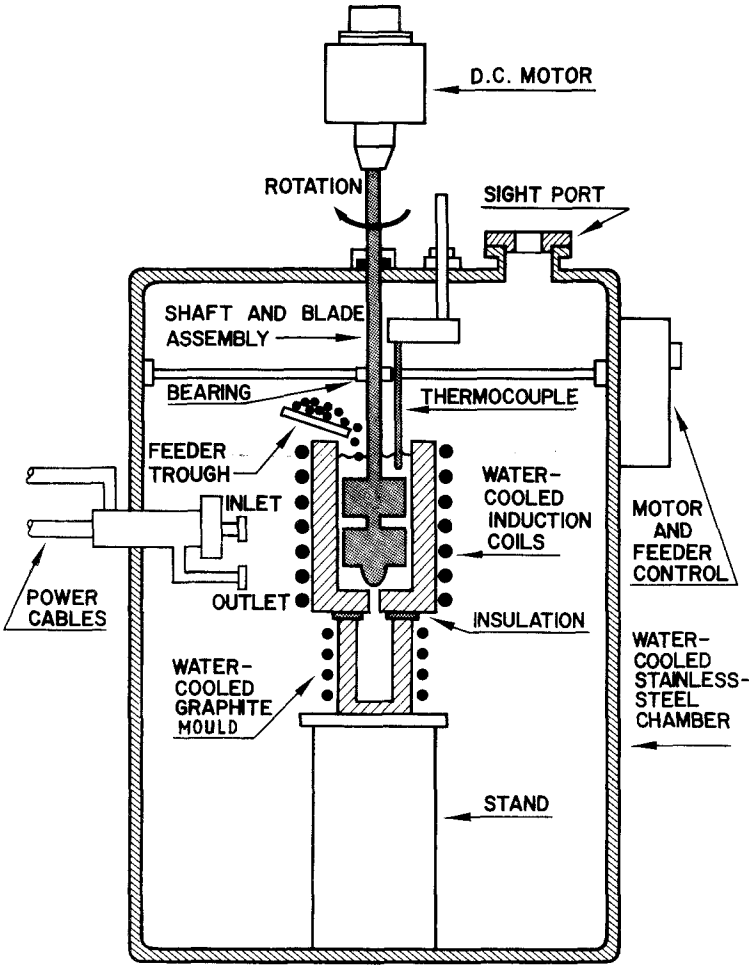

Figure 4 Schematic illustration of the compositing apparatus.

at the base of the shaft below the two blades to complete the assembly.

An alundum crucible (~90 mm in diameter by ~150 mm) with a bottom hole was designed and used in the furance. A tapered graphite insert with a centre hole (25 mm in diameter) was positioned at the bottom of the crucible to allow bottom pouring of the composite. The graphite plug on the blade assembly mates with this insert during the preparation of the composite. This rotating seal prevents leakage of the melt.

The composites are cast in a water-cooled graphite mould, ~ 90 mm in diameter by ~ 125 mm in height, located directly below the crucible assembly. The non-metallic particles are introduced into the alloy slurries by means of a magnetic feeder device with a variable controller to regulate the feed rate. The trough is positioned such that the particles enter the melt between the rotor and the crucible wall.

Approximately 1 kg of aluminium alloy was placed in the system with the blade assembly in place. The chamber was evacuated to a pressure of 0.15 torr using the mechanical pumps only. The alloy was then superheated above its melting temperature and the agitation was initiated as described above. The induction power was gradually lowered until the alloy was 40 to 50% solid, at which time the non-metallic particulates were added to the slurry. The power input was controlled such that the total per cent of solid, non-metals and solid spheroids of the alloy, did not exceed about 50%. The rotation speed of the blade was generally maintained at 240 rpm. Stirring was continued until interface interactions between the particulates and the matrix promoted wetting. The melt was then superheated to above its liquidus temperature and bottom-poured into the graphite mould by raising the blade assembly.

2.2. Shape forming of the composites

The forging apparatus used is shown in Figs 5 and

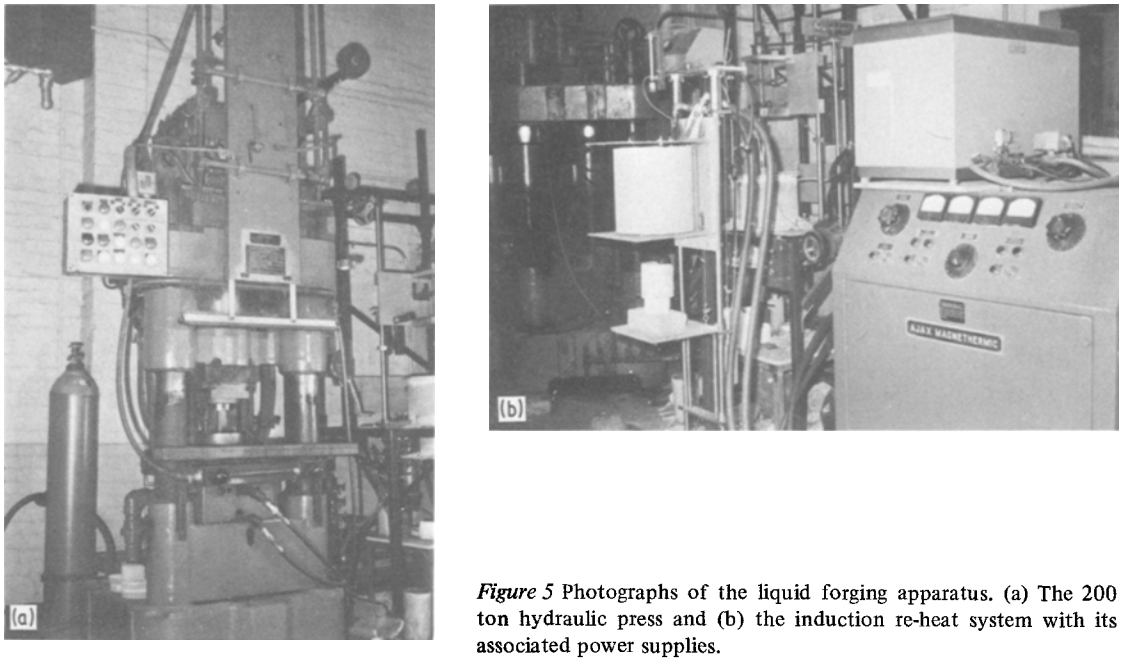

Figure 5 Photographs of the liquid forging apparatus. (a) The 200 ton hydraulic press and (b) the induction re-heat system with its associated power supplies.

6. It consists of a high-frequency induction furnace and power supply (400 V, 15 kW, 3000 Hz) and an automated hydraulic (200 ton) forging press modified to permit shaping and solidification of completely-liquid and partially-solid charge materials under pressure.

The forging dies illustrated in Fig. 7 were sprayed with a thin coating of graphite powder mixed with isopropyl alcohol. A ring insert was placed in the lower die-half to allow fabrication of shapes that would provide material for wear and mechanical testing. The smaller diameter (~80 mm) section was used to study the wear properties and the larger diameter (~115 mm) section was used to examine the mechanical properties of the composites.

The shape-forming sequence of operations was as follows. The cast composites were placed in an alumina crucible (~ 100 mm in diameter and 170 mm in height) and reheated in the induction furnace to a superheat of 50 K. The temperature was closely monitored with a thermocouple in order to prevent overheating. The crucible was then removed from the furnace. The oxide film on top of the melt was skimmed off and the melt was gently stirred mechanically to avoid particle settling. The melt containing the non-metallic particles was then transferred into the lower die-half of the press and the top die was brought down to shape and solidify the composite under an applied pressure of approximately 2×10^8 Pa. The pressure was maintained

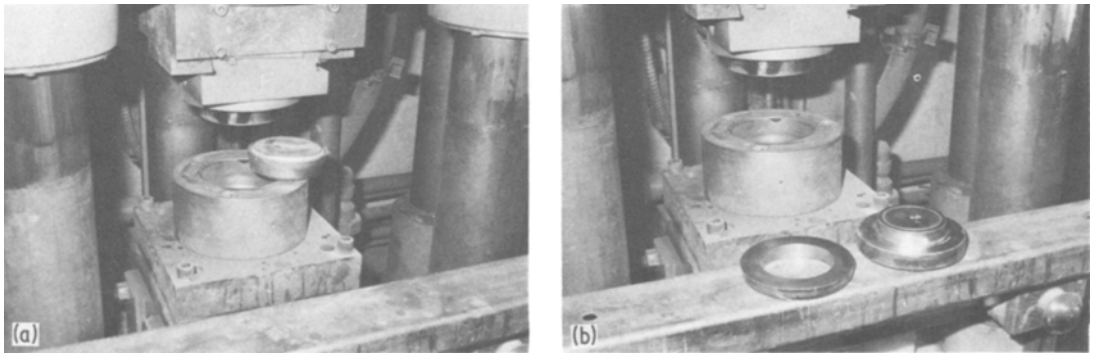

Figure 6 Photographs of the forging die in the hydraulic press and the parts produced. (a) shows a disc-shaped part about 115 mm in diameter and about 40 mm in height. (b) Shows the steel ring insert used in the lower die-half to produce the reduced cross-section disc-shape on the right.

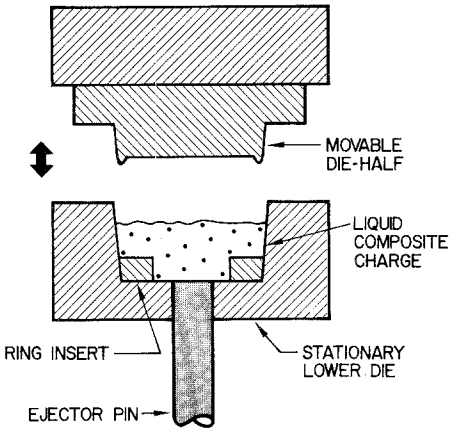

Figure 7 Schematic illustration of the forging dies used in forming of the aluminium-matrix composites in the hydraulic press.

for 90 sec to complete the solidification before the composite was ejected. Solidification in the unheated steel dies under direct applied pressure resulted in a structure free of macroporosity with a relatively homogeneous distribution of the non-metallic particles. Fig. 6b shows a typical shaped composite part produced in this investigation.

2.3. High-volume fraction and dual-layered Composites

In certain applications it may be desirable to have a composite either with a high volume-fraction of non-metals (~0.5) or with a gradation of non-metallic particulates, for example, a wear-resistance surface backed by a ductile matrix. Two similar but slightly different techniques were developed for the production of such composites.

In the first process a porous ceramic filter was used to remove a portion of the matrix liquid during the forming operation. This 20 mm thick ceramic filter* was first located in the bottom of the lower die. A 3 mm thick layer of 150 μm-sized Al_2O_3 particles was spread uniformly on the top of the filter. This was carried out to prevent infiltration of particles of the composite into the porous filter. The composite was superheated to 50 K above its liquidus temperature, transferred to the lower die-half and solidified under pressure, as previously described. Fig. 8 shows a schematic illustration of the experimental set-up prior to and after the forming operation. This process was successful in producing high volume-fraction composites. It should be noted that a thin layer of matrix of

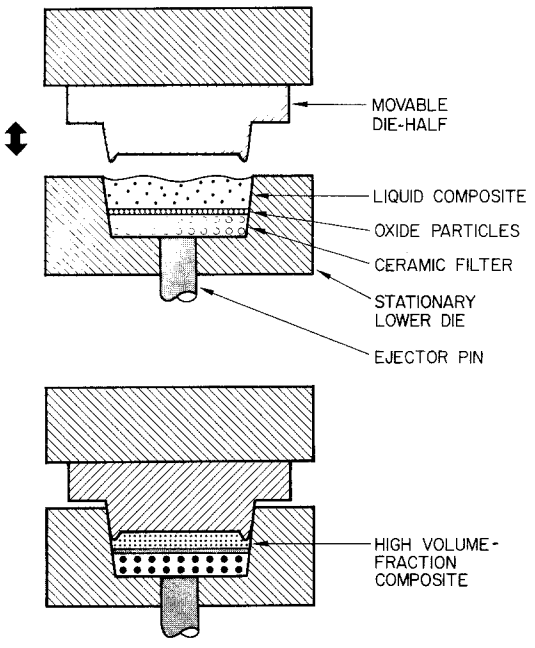

Figure 8 Schematic illustration of the die set-up used to fabricate high volume-fraction composites of aluminium alloys.

about 2 to 3 mm in thickness, devoid of non-metallic particulates, was consistently noted at the top of the composites following this operation.

Composites with a variable concentration of non-metallic particles were readily produced using a second technique. The procedure followed was to sequentially add the composite and a superheated liquid melt devoid of any particles into the lower die-half prior to pressurization. The viscous composite, about 6.0 mm in thickness, remains at the bottom of the disc-shaped part if the matrix alloy is added gently by means of a coated stainless-steel trough. Composite parts produced in this way contain a sharp discontinuous non-metallic composition gradient.

2.4. Composite compositions and evaluation techniques

Table I gives a list of the composites fabricated. The disc-shaped parts, Fig. 9, were sectioned with a diamond saw to prepare specimens for friction and wear and mechanical behaviour studies. The friction and wear properties were investigated on a pin-on-disc-type machine, see Fig. 10.

Standard round tensile specimens of 6.35 mm gauge diameter and 25.4 mm gauge length were

*Selee, A product of Consolidated Aluminium.

TABLE I Sample identification and composition of the composites fabricated and tested

Specimen identification	Matrix alloy	Particles charged*	
		Size (μm)	Amount charged (wt %)
2024	2024	–	–
2024–10 wt %(1 μm Al_2O_3)	2024	1	10.0†
2024–2 wt %(5 μm Al_2O_3)	2024	5	2.0†
2024–5 wt %(5 μm Al_2O_3)	2024	5	5.0†
2024–20 wt %(5 μm Al_2O_3)	2024	5	20.0†
2024–5 wt %(16 μm Al_2O_3)	2024	16	5.0†
2024–20 wt %(16 μm Al_2O_3)	2024	16	20.0†
2024–20 wt %(63 μm Al_2O_3)	2024	63	20.0†
2024–20 wt %(142 μm Al_2O_3)	2024	142	20.0†
2024–30 wt %(142 μm Al_2O_3)	2024	142	30.0†
2014	2014	–	–
2014–2 wt %(1 μm Al_2O_3)	2014	1	2.0†
2014–5 wt %(1 μm Al_2O_3)	2014	1	5.0†
2014–2 wt %(5 μm Al_2O_3)	2014	5	2.0†
2014–5 wt %(5 μm Al_2O_3)	2014	5	5.0†
2014–5 wt %(16 μm Al_2O_3)	2014	16	5.0†
2014–5 wt %(63 μm Al_2O_3)	2014	63	5.0†
2014–20 wt %(16 μm Al_2O_3)	2014	16	20.0†
2014–5 wt %(16 μm SiC)	2014	16	5.0†
2014–20 wt %(16 μm SiC)	2014	16	20.0†
201	201	–	–
201–5 wt %(5 μm Al_2O_3)	201	5	5.0†

*Al_2O_3: Unfused Alumina (plate-like, sharp morphology).
†Specimens subjected to wear tests.

tested with an Instron testing machine at a strain rate of 1.25 mm min^{-1}.

Evaluated-temperature tensile tests were also performed with the same specimen dimensions as used in the room-temperature tests. An MTS mechanical testing system with a high-temperature furnace (1275 K of maximum working temperature) mounted on the load frame was used. The tensile specimens were heated up to a temperature of 525 K and held at this temperature for 15 min to allow for a uniform temperature distribution throughout the specimen. Testing proceeded subsequently at a cross-head speed of 1.0 mm min^{-1}.

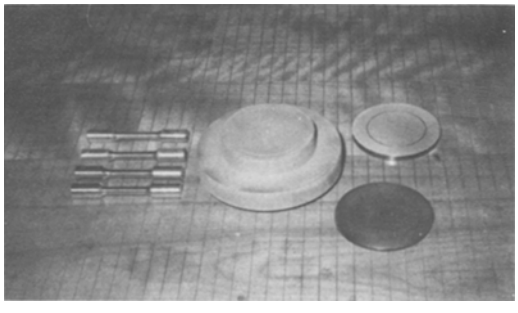

Figure 9 Photograph showing an aluminium-matrix composite in the as-forged condition with sections removed and machined from a similar part for wear and tensile tests.

2.5. Wear measurements

The friction and wear measurements were carried out on the pin-on-disc-type machine, shown in Fig. 10, which was built for this investigation. It is similar to the machine described by Burwell and Strange [14].

The circular disc with the specimen holders is driven by a variable speed direct current motor. The speed of the motor was varied on different wear track diameters such that a constant speed of 100 mm sec^{-1} could be maintained throughout all the tests. The normal force is imparted by placing weights on the rider (pin) which is attached to the end of the counter-weighted flexible arm shown in Fig. 10. An aluminium dynometer ring about 9 cm in diameter, about 2 cm in width and about 0.12 cm in thickness, with strain gauges attached on the inside and outside of the ring, is used to measure the bending strain due to the friction force. The signal, which is obtained through a differential amplifier, is recorded on a Gould strip chart recorder. The average coefficient of friction is then calculated from this data.

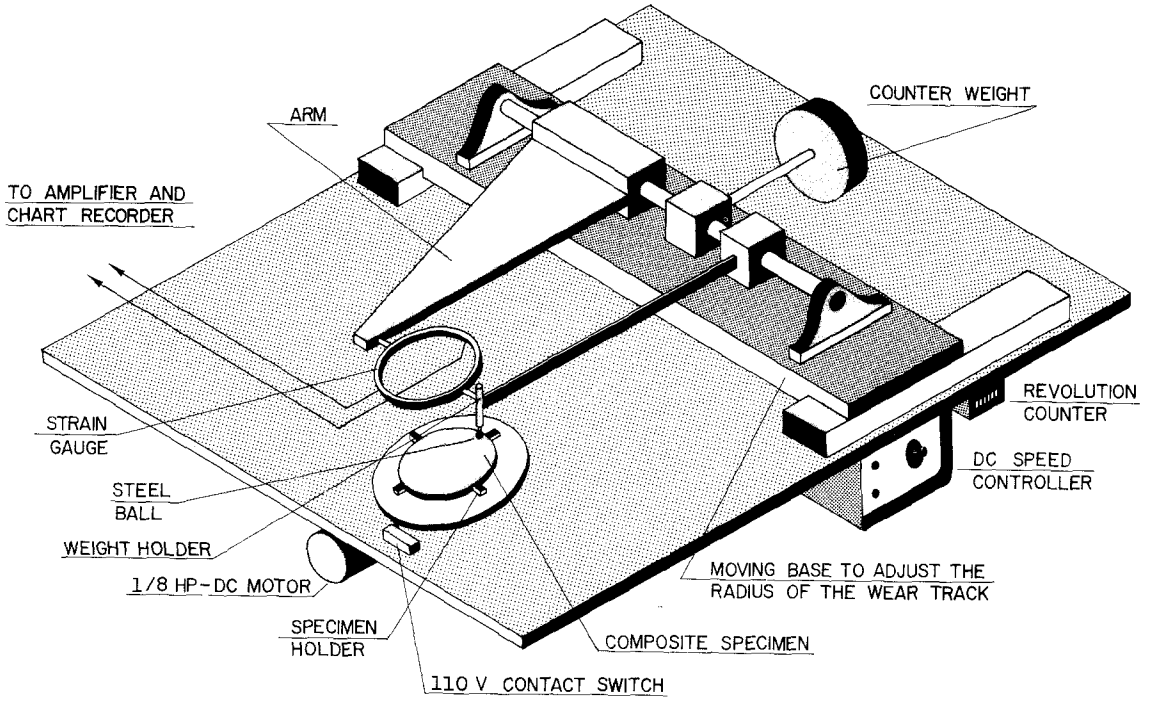

Figure 10 Schematic illustration of the wear-test machine.

The rider (pin) consists of a vertical-treaded (~ 6.3 mm diameter) rod which fits at one extremity of the dynamometer ring. A 6.4 mm diameter AISI type E-52100 ball-bearing* was attached to the end of the pin with epoxy. A new ball-bearing was used at the beginning of each test.

The composite specimens, about 80 mm in diameter and 2 to 4 mm in thickness were removed from the smaller section of the shaped forging shown in Fig. 9. Two disc-shaped specimens were removed with a diamond saw from each forging. These were machined flat and polished with 600 grit SiC paper prior to each test. All the specimens were tested in the as-cast condition with no heat treatment.

The wear test consisted of weight loss and coefficient of sliding friction measurements against the ball-bearings noted above. All tests were carried out under dry-sliding conditions. Prior to each test both the disc and the bearing were de-greased with acetone. The weight-loss was measured with an accuracy of ± 0.1 mg after every 100 metres of sliding.

Wear mechanisms were studied by examination of specimens polished with 6 μm diamond compound followed by 0.3 μm Al_2O_3 particles prior to each test. The wear tests were run from a few cycles up to 2000 metres. The tracks were examined with optical and scanning electron micro-scopes.

3. Results and discussion

The disc-shaped composites produced were sectioned, their structures were examined by scanning electron microscope techniques and their mechanical, friction and wear properties were determined.

3.1. Microstructure of the composites

Representative microstructures of the liquid-forged disc-shaped composites are shown in Figs 11 to 13. A high weight per cent addition of coarse Al_2O_3 particles generally resulted in homogeneous distributions of the non-metals in the aluminium alloy matrices. Note the uniform distribution of the particles in Figs 11 to 13 as well as the absence of voids in the surrounding matrix. The latter is attributed to solidification under the high direct applied pressure in the forging press. Relatively uniform distributions were observed in almost all the composites produced when the weight per cent and size

*The ball-bearing used is of Anti-Friction Bearing Manufacturer's Association Grade 25.

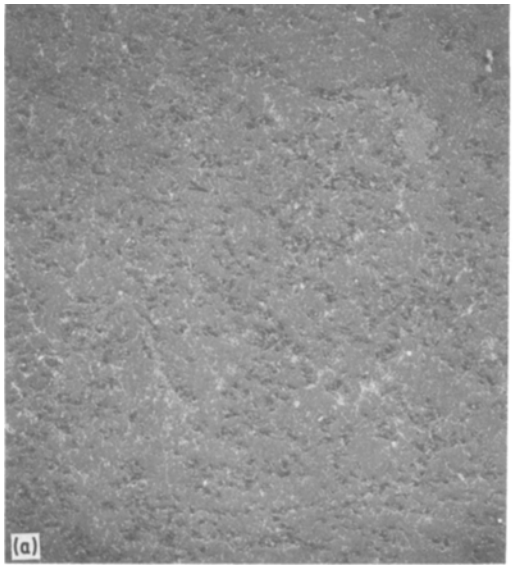

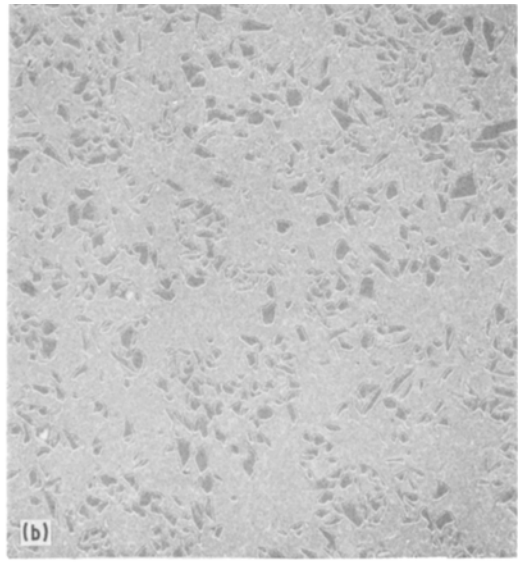

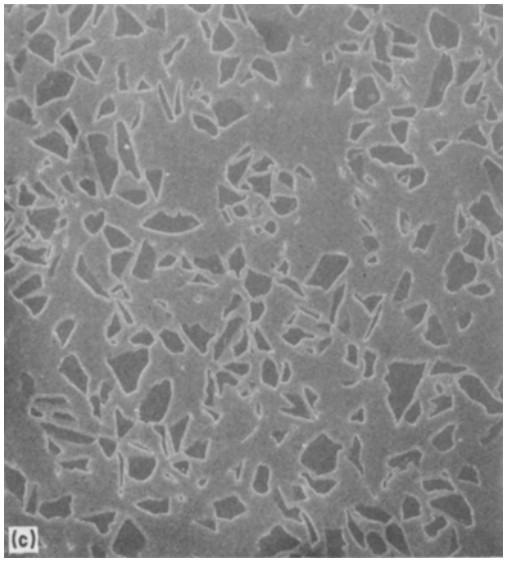

Figure 11 SEM photomicrographs of liquid-forged composites of aluminium alloys containing 20 wt% Al_2O_3 particles, 40 ×. (a) 16 μm particles in a 2014 aluminium alloy, (b) 63 μm particles in a 2024 aluminium alloy, (c) 142 μm particles in a 2024 aluminium alloy.

of the non-metallic additions were 5 per cent and or more and 5 μm or larger, respectively.

On the other hand, significant particle clustering (formation of segregated regions of concentrated particles surrounded by regions of matrix devoid of particles) was observed when the particle additions were in the 1 μm size range. Attempts to break-up these clusters by mild mechanical agitation of the remelted composites, prior to forging, were not successful. Severe agitation was avoided because it causes air entrapment in the composite. It is postulated that the clusters form during composite fabrication, when the fine particulates are added to the alloy slurry, and are entrapped in the liquid matrix surrounding the primary solid particles. Agitation of the reheated composites prior to forging, while not effective in breaking up the clusters, did ensure a uniform distribution of the clusters themselves in the shaped part.

Interface interactions between Al_2O_3 and aluminium matrices during the fabrication of composites using mechanical agitation have been previously investigated [4, 5]. The formation of $MgAl_2O_4$ and $CuAl_2O_4$ spinels and other interactions [4] between alumina fibres and aluminium matrices has already been discussed. Close examination of these interfaces using Auger and electron diffraction techniques [5] has verified the earlier findings. Particulate composites produced in the present investigation revealed excellent intimate bonds between the Al_2O_3 particles and the various matrices. All three matrices contain magnesium and copper as alloy element additions. Thus, it is postulated that interactions similar to those noted above are responsible for bonding at the interfaces.

Fig. 14 shows optical microscope views of a dual-layered, high volume-fraction composite of an 2024 aluminium alloy made using the special ceramic filter and oxide particles shown in Fig. 8. The oxide particles, 142 μm in size, were identical to those put in the alloy matrix. These were sprinkled on top of the filter in order to prevent the

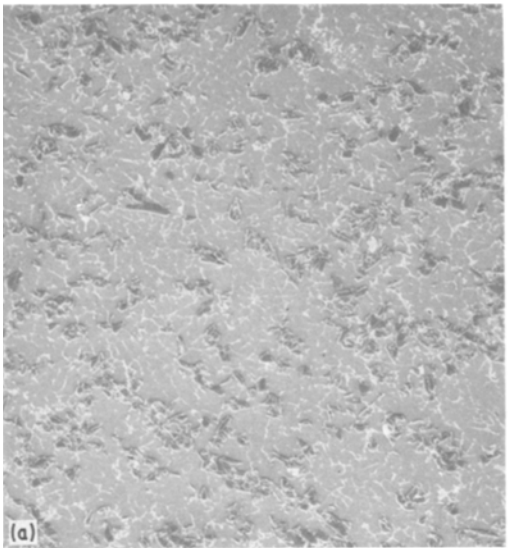

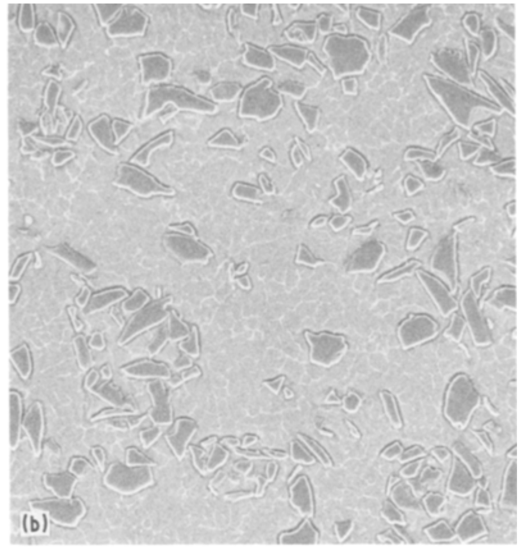

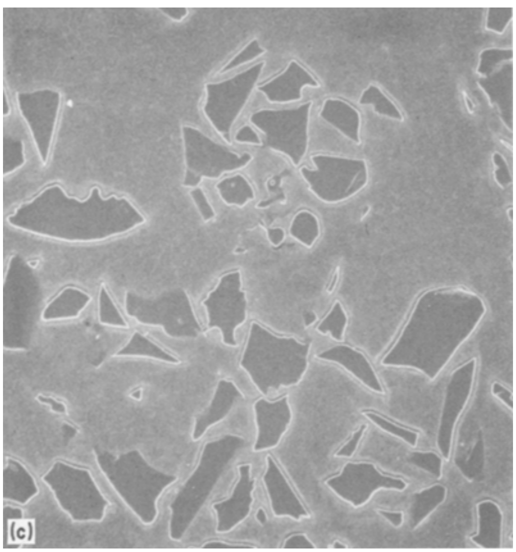

Figure 12 SEM photomicrograph of liquid-forged composites of aluminium alloys containing 20 wt% Al_2O_3 particles, 90 ×. (a) 16 μm particles in a 2014 aluminium alloy, (b) 63 μm particles in a 2024 aluminium alloy, (c) 142 μm particles in a 2024 aluminium alloy.

particles in the composite itself from infiltrating the ceramic filter. Thus, the lower extremity of the structure shown in Fig. 14 consists of infiltrated Al_2O_3 particles which are not completely wetted by the matrix alloy.This oxide layer was separated from the dual-layered composite by means of a diamond saw. Thus, the final product was a disc-shaped part composed of two layers, an Alloy 2024 matrix followed by a composite containing approximately 30 wt% of 142 μm-sized Al_2O_3 particles. It is postulated that composites thus produced would be used in applications where exceptional wear properties on a given surface are desired in combination with a relatively ductile internal microstructure.

The other technique, i.e., the dual-layered technique described in the procedure, was equally successful in producing tailored inhomogeneous composites such as the one discussed above. In the latter approach introduction of the superheated matrix alloy on top of the remelted composite had to be carefully controlled to avoid intermixing of the two. Dual-layer composites like that shown in Fig. 14b were successfully produced in this way.

Finally, other processing options such as cen-

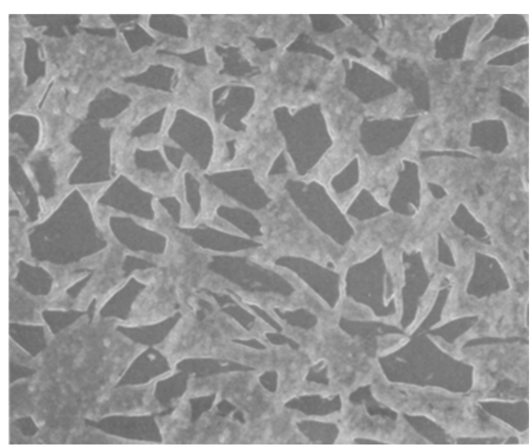

Figure 13 SEM photomicrographs of a liquid-forged composite of 2024 aluminium alloy containing 30 wt% 142 μm-sized Al_2O_3 particles, × 74.

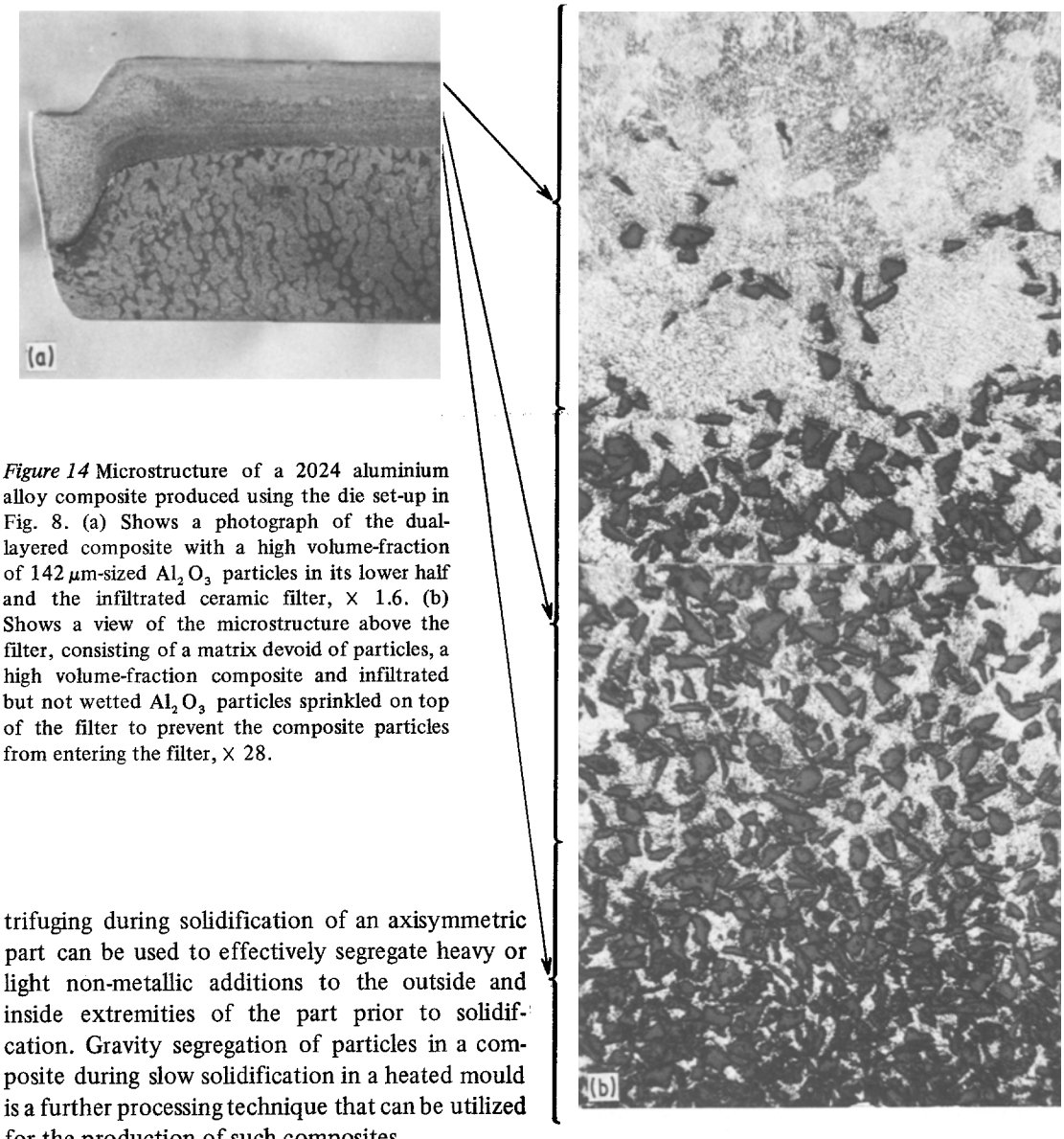

Figure 14 Microstructure of a 2024 aluminium alloy composite produced using the die set-up in Fig. 8. (a) Shows a photograph of the dual-layered composite with a high volume-fraction of 142 μm-sized Al_2O_3 particles in its lower half and the infiltrated ceramic filter, × 1.6. (b) Shows a view of the microstructure above the filter, consisting of a matrix devoid of particles, a high volume-fraction composite and infiltrated but not wetted Al_2O_3 particles sprinkled on top of the filter to prevent the composite particles from entering the filter, × 28.

trifuging during solidification of an axisymmetric part can be used to effectively segregate heavy or light non-metallic additions to the outside and inside extremities of the part prior to solidification. Gravity segregation of particles in a composite during slow solidification in a heated mould is a further processing technique that can be utilized for the production of such composites.

3.2. Mechanical properties

The main objective in the production of the aluminium-matrix composites and their subsequent shape-forming is for the use as net or near net-shaped components in applications requiring exceptional wear behaviour. However, it is essential that such composite components, or surfaces in the case of intentionally segregated composites, possess predictable minimum acceptable mechanical properties. The room- and high-temperature tensile properties of the composites reported below were determined to satisfy the latter requirement.

The disc-shaped composites were sectioned with a diamond saw into rectangular blanks for subsequent machining of the tensile test bars shown in Fig. 9. All the composite specimens and the matrix alloys shaped in an identical manner were tensile tested in the heat-treatment T-4 (solutionized and room-temperature aged) condition.

The average measured room-temperature tensile properties of both the composites and the matrix alloys are listed in Table II. The tensile properties and ductilities of even the matrix alloy are lower than those reported in an earlier study [15]. This is attributed to the fact that in the earlier work the alloys were degassed and protected with nitrogen prior to the forging operation. Oxide entrapment was thus minimized in the forgings.

TABLE II Room-temperature mechanical properties of liquid-forged composites and matrix alloys heat-treated to T4-condition

Specimen	Ultimate tensile strength, kg/mm^2 (kg mm^{-2})	0.2% offset yield strength (kg mm^{-2})	Elongation (%)	Reduction area	Ducility, ($\ln A_o/A_f$)
2024	38.8	26.8	8.2	6.3	0.065
2024–10 wt %(1 μm Al_2O_3)	21.3	–	0.6	1.6	0.016
2024–2 wt %(5 μm Al_2O_3)	31.9	24.0	2.8	4.0	0.041
2024–5 wt %(5 μm Al_2O_3)	34.5	24.9	3.4	4.8	0.050
2024–20 wt %(5 μm Al_2O_3)	16.5	–	0.5	0.8	0.008
2024–5 wt %(16 μm Al_2O_3)	32.5	25.9	2.2	4.0	0.041
2024–20 wt %(16 μm Al_2O_3)	13.9	–	0.4	0.0	0.000
2024–20 wt %(142 μm Al_2O_3)	20.7	–	0.3	0.0	0.000
2024–30 wt %(142 μm Al_2O_3)	15.4	–	0.2	0.0	0.000
2014	32.0	21.3	7.0	7.1	0.073
2014–2 wt %(1 μm Al_2O_3)	25.4	20.2	1.6	3.9	0.033
2014–5 wt %(1 μm Al_2O_3)	22.4	20.8	1.0	1.6	0.016
2014–2 wt %(5 μm Al_2O_3)	34.3	23.5	5.7	6.3	0.065
2014–5 wt %(5 μm Al_2O_3)	31.9	22.0	5.1	7.1	0.073
2014–5 wt %(16 μm Al_2O_3)	30.9	22.5	4.2	4.0	0.040
2014–5 wt %(63 μm Al_2O_3)	29.6	21.4	3.4	6.3	0.065
201	34.1	18.9	14.0	21.0	0.237
201–5 wt %(5 μm Al_2O_3)	27.7	21.6	2.6	3.6	0.040

Furthermore, the higher volume-fraction composites were very brittle and possessed low tensile properties. For example, the 20 wt% Al_2O_3 composites in the T-4 condition had an average tensile strength of 16.5 kg mm^{-2} and a corresponding elongation of approximately 0.4. The low ductilities in these specimens can be attributed to the large number of block-like particles with sharp corners which make the composites prone to localized crack initiation and propagation. Finally, the lower volume-fraction composites containing relatively homogeneous distributions of fine Al_2O_3 retain reasonable tensile properties comparable to, and in some cases exceeding, the yield strength of the matrix alloy solidified under identical conditions. For example, note the tensile data on 2014 and 201 alloy composites containing 5 wt% of 5 μm-sized Al_2O_3 particles. These latter observations are in accord with those reported by Sato *et al.* [2] for hot-extruded composites of aluminium alloys prepared in a similar manner.

The results of Edelson and Baldwin [3] reviewed earlier and reported in Fig. 2 show that ducility, as measured by $\ln(A_o/A_f)$, continuously decreases with volume-fraction of particulate additions and appears to be independent to particle size. The data in Table II are plotted in a similar manner in Fig. 15. The trend established between ductility and volume-fraction of Al_2O_3 is similar to that reported earlier [3]. However, the ductilities of the present study appear to fall far lower than those in the curve produced by Edelson and Baldwin [3], also shown in Fig. 15. It is postulated that their higher ductilities can be attributed to the very ductile, forgiving copper matrix used.

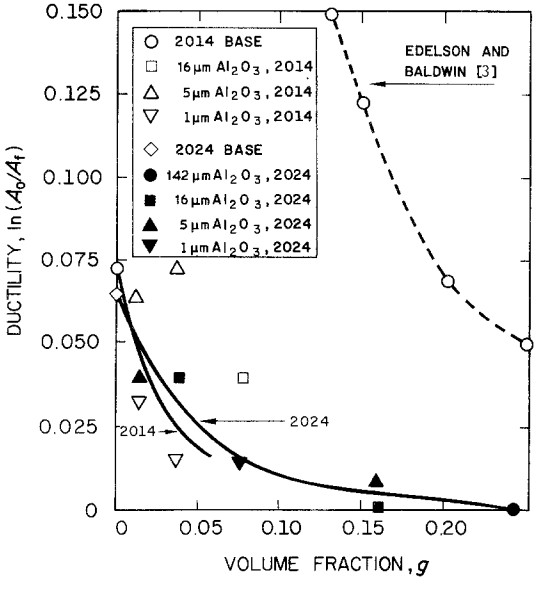

Figure 15 Ductility plotted against volume-fraction of Al_2O_3 particles in a number of aluminium alloy composites liquid-forged into shape and heat-treated to a T-4-condition.

TABLE III Elevated temperature (525 K) properties of liquid-forged composites and matrix alloys heat-treated to T4-condition

Specimen	Ultimate tensile strength (kg/mm^{-2})	Elongation (%)	Reduction area (%)
2024	26.5	10.0	10.9
2024–10 wt %(1 μm Al_2O_3)	9.0	1.4	2.4
2024–5 wt %(5 μm Al_2O_3)	24.2	2.0	2.4
2024–5 wt %(16 μm Al_2O_3)	24.0	2.5	3.2
2014	23.5	9.0	10.2
2014–2 wt %(1 μm Al_2O_3)	10.0	4.5	4.7
2014–5 wt %(1 μm Al_2O_3)	20.0	3.0	3.9
2014–2 wt %(5 μm Al_2O_3)	16.8	7.5	7.1
2014–5 wt %(5 μm Al_2O_3)	21.0	2.5	4.0
2014–5 wt %(16 μm Al_2O_3)	18.5	3.0	6.3
2014–5 wt %(63 μm Al_2O_3)	21.2	5.0	7.0
201	25.2	21.0	19.7
201–5 wt %(5 μm Al_2O_3)	20.9	6.5	7.0

The measured elevated-temperature (525 K) tensile properties of the matrix alloys and the composites are listed in Table III.

The higher volume-fraction specimens were not tested due to their poor room-temperature tensile properties. Small improvements in the elongation were observed with ultimate strength values decreasing by from 8 to 15 $kg\,mm^{-2}$.

3.3. Friction and wear behaviour

The wear tests were carried out on the apparatus shown in Fig. 10. The procedure used was that previously described. Photographs of discs removed and machined for use in the wear-test machine are shown in Fig. 16. The wear tracks made by the 52100 ball-bearing can be seen on three of the discs. The uniform distribution of the non-metals is readily noted in the discs containing the coarser Al_2O_3 particles, see Fig. 16c and d. All the tests were carried at a constant sliding velocity of 10 cm sec^{-1}. The weight-loss in each specimen was determined after a given sliding distance. The wear mechanisms were established by examination of both the pin and the wear track.

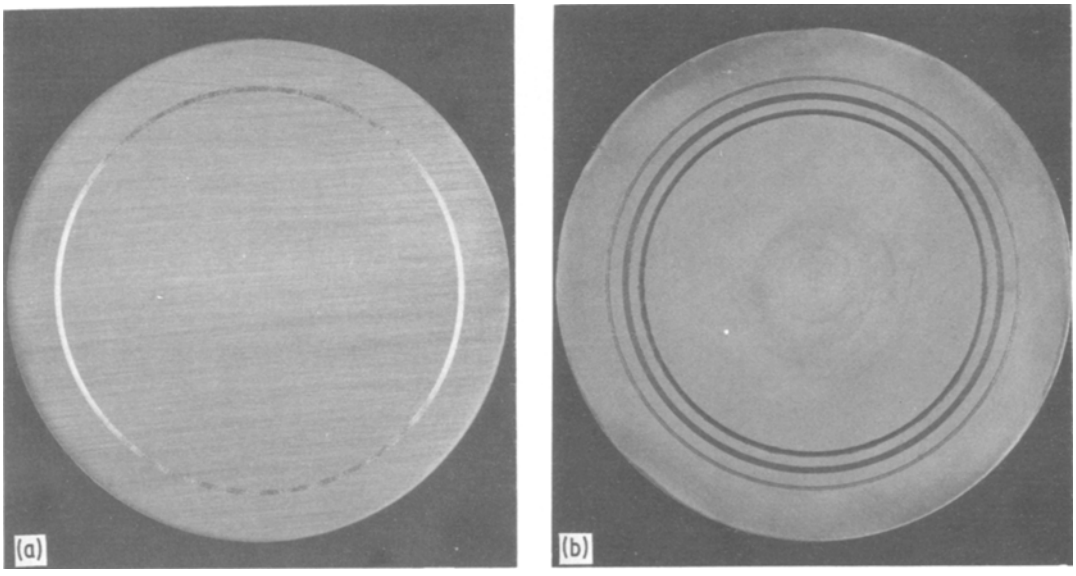

Figure 16 Photographs of wear specimens of a liquid-forged matrix and composites, × 0.86. Wear tracks can be noted on three of the discs. (a) 2014 aluminium alloy matrix, (b) 2014 aluminium alloy containing 20 wt % 16 μm-sized SiC particles, (c) 2024 aluminium alloy containing 20 wt % 63 μm-sized Al_2O_3 particles, (d) 2024 aluminium alloy containing 20 wt % 142 μm Al_2O_3 particles.

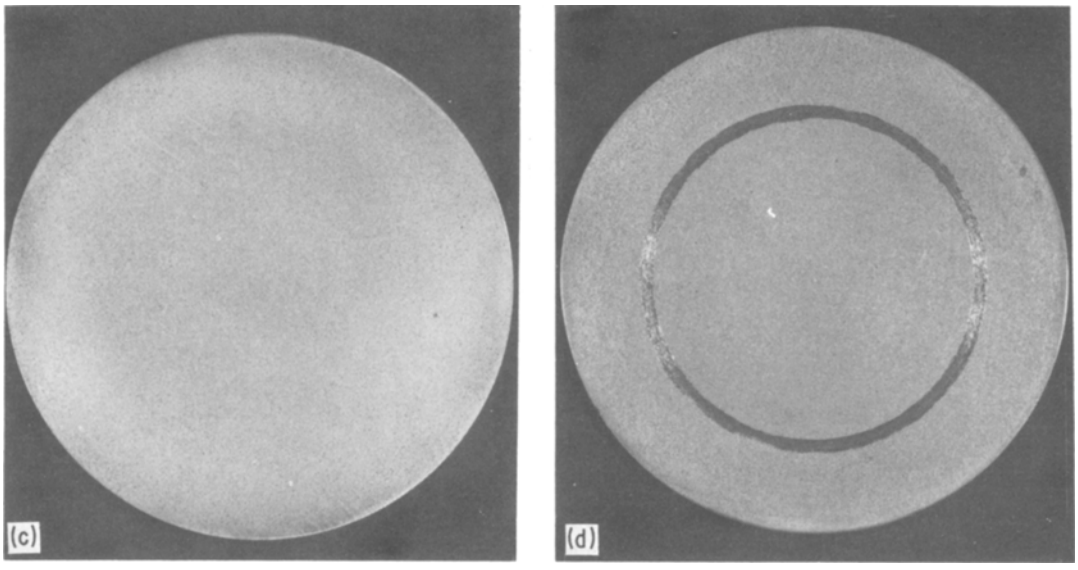

Figure 16 Continued

3.3.1. Measured weight-loss

Measured weight-loss (and volume-loss) against sliding distance plots for a number of the composites determined under different applied loads are shown in Figs 17 to 19. In order to establish the effect of non-metallic additions on the wear behaviour of the composites each figure contains the average weight-loss plotted against the sliding distance data of the matrix alloys liquid-forged identical conditions.

In general, the data in Figs 17 to 19 show that for any given specimen the weight- or volume-loss continuously increases with increasing sliding distance. Fig. 17 displays the wear of 2024 aluminium alloy – Al_2O_3 particle composites under an applied normal load of 50 g. The trends established in Fig. 17 are, first, that the introduction of the hard non-metallic particles reduces the weight-loss at a given sliding distance and, second, that the weight-loss at a given sliding distance decreases with increasing weight per cent and size of Al_2O_3 particles.

Fig. 18 shows wear data obtained under different applied load conditions. The two composites contain different weight per centages of 16 μm-size SiC particles. In each composite, weight-loss increases with increasing applied load, for example, in the composite containing 5 wt % of SiC particles a four-fold increase in applied load, from 50 to 200 g, results in a weight-loss which is higher than the matrix alloy. Again, as in Fig. 17, increasing the amount of the non-metallic addition results

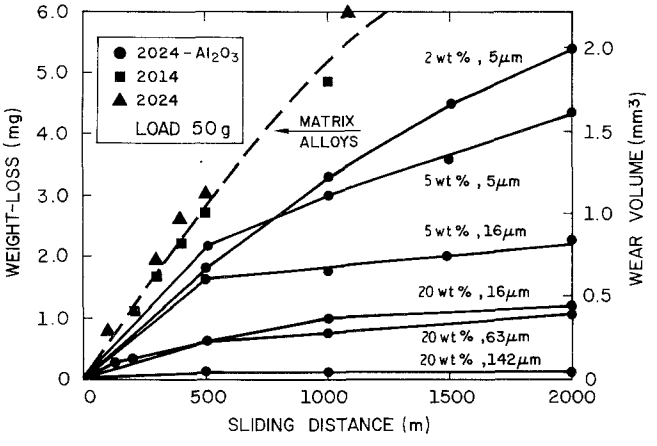

Figure 17 Weight-loss plotted against sliding distance of aluminium-matrix alloys 2014 and 2024 and composites of 2024 containing different weight percentages of four different-sized Al_2O_3 particles. Applied load on the rider (pin) was 50 g.

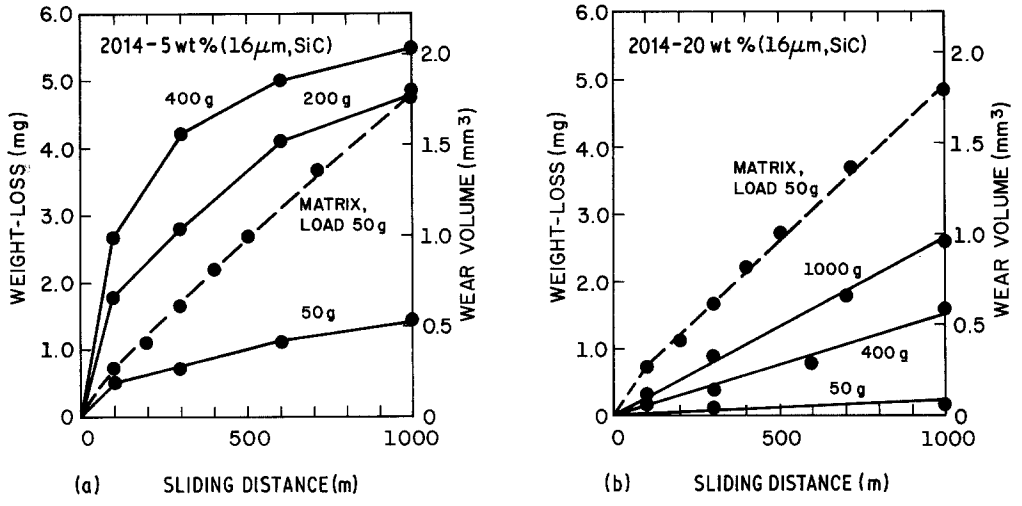

Figure 18 The effect of applied load on weight loss plotted against sliding distance of aluminium-matrix alloy 2014 and composites of alloy 2014 containing (a) 5 wt % and (b) 20 wt % 15 μm-sized SiC particles.

in reduced wear when all other variables are kept constant.

Attempts were made to compare the wear behaviour of aluminium alloys containing Al_2O_3 particles and SiC particles, see Fig. 19. As previously noted, the 2014 and 2024 matrix alloys showed almost similar wear behaviour under identical test conditions. Therefore, it is postulated that the differences in wear behaviour noted in Fig. 19 can be ascribed to the non-metallic additions. The data show that the SiC particles (Vickers hardness of 2600) are more effective than the Al_2O_3 particles (Vickers hardness of 1800) in resisting wear.

Figs 20 and 21 show the measured coefficients of sliding friction as a function of composite composition and applied load. The data show that, in general addition of the non-metallic particles reduced the coefficients of friction. Beyond this general observation, no clear trends relating composition or tests conditions to the coefficient of sliding friction could be established.

3.3.2. Wear mechanisms

A general observation made in this portion of the investigation was that with increasing additons of non-metals to the aluminium matrices the wear mechanism changed from a purely adhesive to mixed mode of oxidative–abrasive wear. The latter resulted in a corresponding wear of the steel ball-bearing. Figs 22 and 23 show the microstructures of a pure matrix alloy, various composition composites and the corresponding ball-bearing pins. Fig. 22a shows the adhesive wear of the aluminium

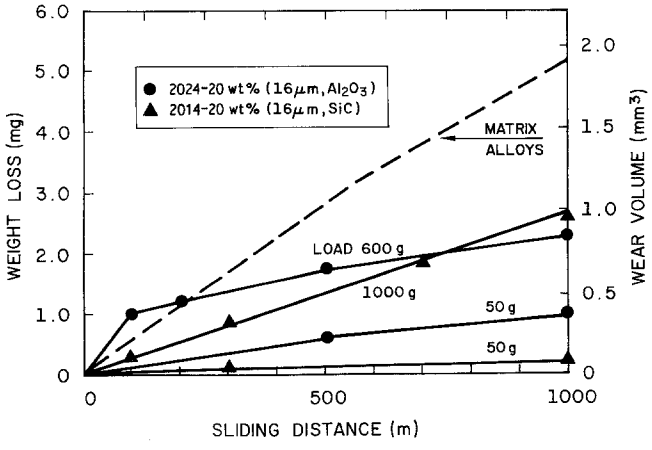

Figure 19 Comparison of the wear behaviour of composites containing SiC and Al_2O_3 particles.

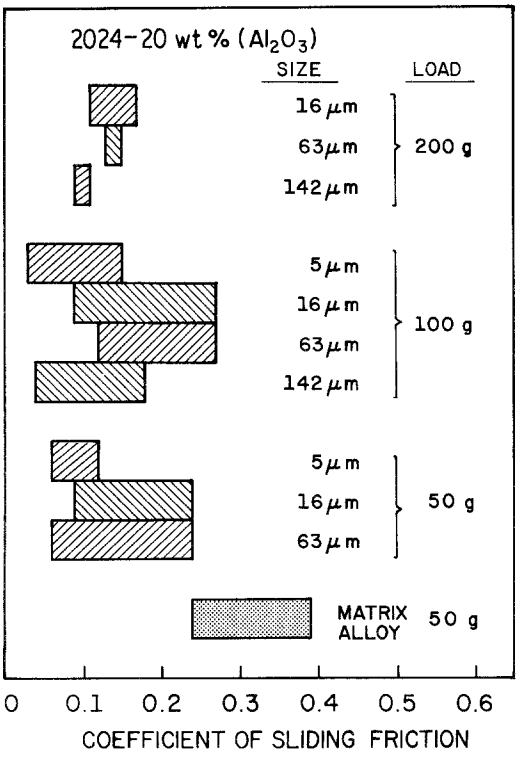

Figure 20 Average measured coefficient of sliding friction of aluminium-matrix alloy 2024 and composites of the alloy containing 20 wt % of different-sized Al_2O_3 particles.

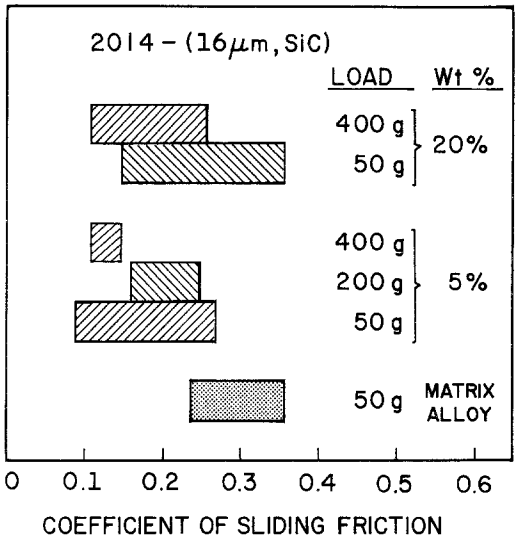

Figure 21 Average measured coefficient of sliding friction of aluminium-matrix alloy 2014 and composites of the alloy containing 5 and 20 wt % 15 μm-sized SiC particles.

alloy 2014. Metal transfer to the pin in this experiment is shown in Fig. 23a. The addition of 5 wt % of 16 μm-sized Al_2O_3 particles appears to reduce both the plastic flow in the matrix and the metal transfer to the pin, see Figs 22b and 23b. When 20 wt % of Al_2O_3 and SiC particles are added to aluminium matrices a dramatic change in the wear mechanism is noted, see Figs 22c and 22d and 23c and 23d. First, the pin again appears to be riding on the particles and, second, there is evidence of an oxide layer on the worn surface of the composites while the pin itself has suffered a purely abrasive wear.

The flow of the matrix over the non-metallic particles is illustrated in Fig. 24. Fig. 24 shows sequences of the microstructure of the wear track of a high non-metal-content (20 wt % of 142 μm Al_2O_3) composite. The applied load in this experiment was 200 g. The microstructures reveal that, initially, the steel ball-bearing was essentially riding on the Al_2O_3 particles. Subsequently, beginning after approximately 25 revolutions, either the particles were pushed into the matrix and/or the matrix covered the particles due to plastic flow in the direction of sliding. A second observation made is that, while some of the particles appear to have fractured either during the composite fabrication and shape-forming or during the wear test, there appears to be no particle pull-out from the matrix even after 2000 revolutions.

Increasing the applied load from 200 to 1000 g on the 20 wt % non-metal-containing composites appeared to change the wear mechanism to a purely abrasive one on both the disc and the pin. While some fine debris are noted, especially on the pin, oxidation of the disc is significantly less than that observed at lower loads, see Fig. 25. Correspondingly, significant wear of the pin areas was noted, see Fig. 25c and 25d.

4. Conclusions

(a)A technique for the fabrication of aluminium-matrix alloy composites containing particulate additions of Al_2O_3 and SiC particles, in the size range of 1 to 142 μm was investigated. The technique uses the special rheological behaviour of partially-solid vigorously-agitated alloy slurries to entrap the particulate additions until interface interactions promote wetting.

(b) Homogeneous additions of the particles in shaped components produced in a forging apparatus were readily obtained except for the very small, 1 μm-sized particles which clustered during the compositing step.

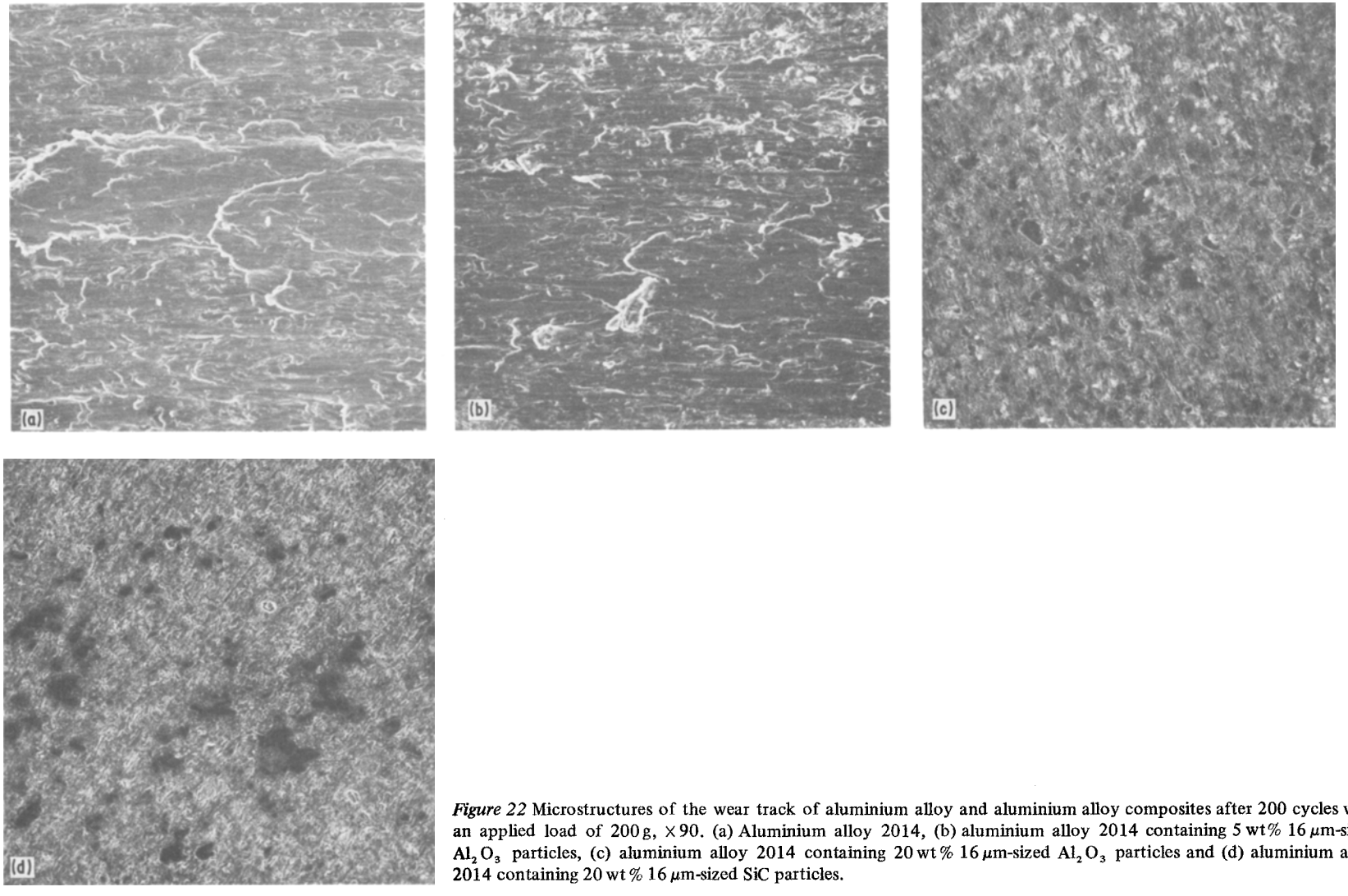

Figure 22 Microstructures of the wear track of aluminium alloy and aluminium alloy composites after 200 cycles with an applied load of 200 g, ×90. (a) Aluminium alloy 2014, (b) aluminium alloy 2014 containing 5 wt% 16 μm-sized Al_2O_3 particles, (c) aluminium alloy 2014 containing 20 wt% 16 μm-sized Al_2O_3 particles and (d) aluminium alloy 2014 containing 20 wt% 16 μm-sized SiC particles.

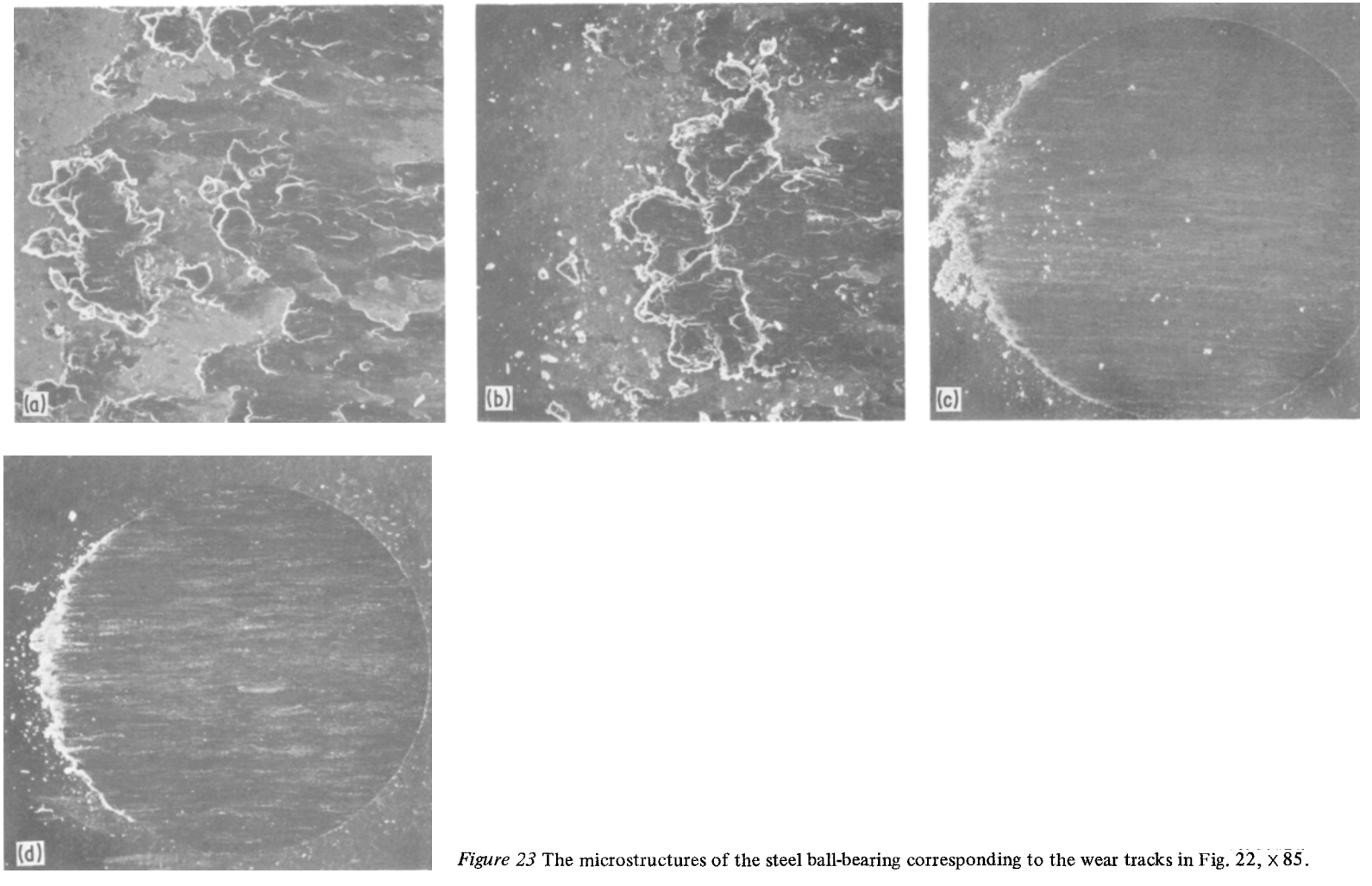

Figure 23 The microstructures of the steel ball-bearing corresponding to the wear tracks in Fig. 22, × 85.

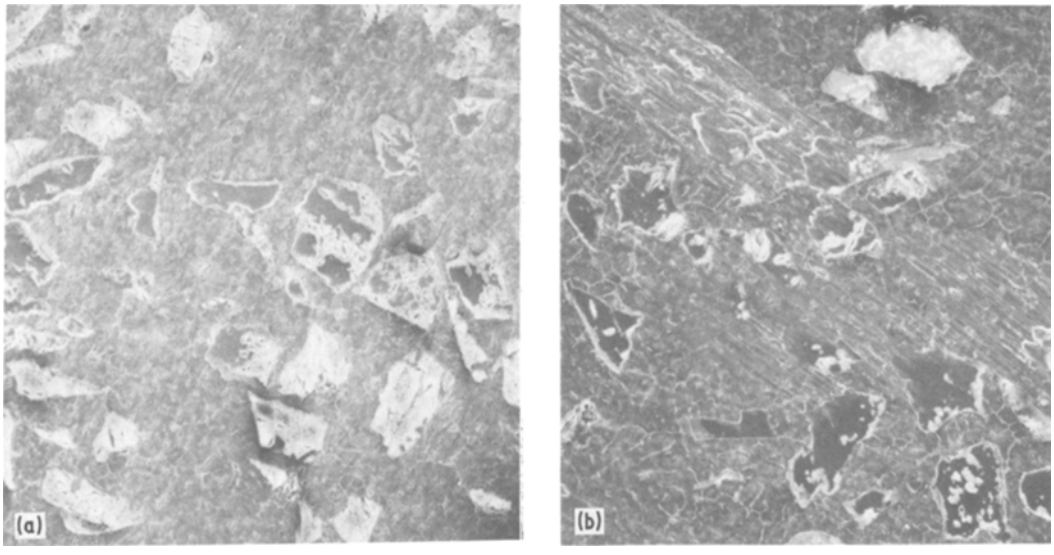

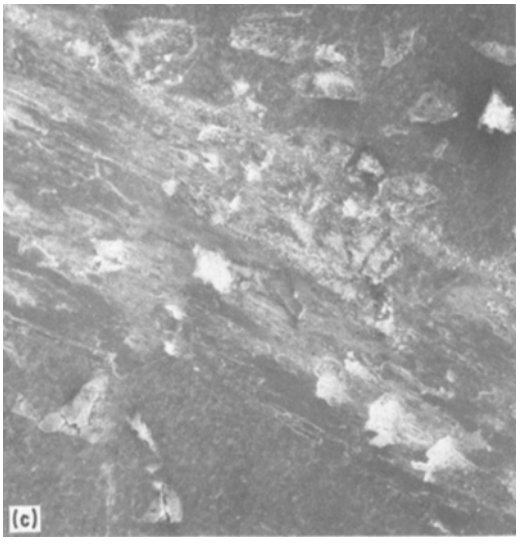

Figure 24 Microstructures of the wear-track of an aluminium alloy 2024 containing 20 wt% 142 μm-sized Al_2O_3 particles, × 93. Sliding velocity and load were 100 m sec^{-1} and 200 g, respectively. (a), (b) and (c) show the microstructures afte 15, 35 and 2000 revolutions, respectively.

(c) Methods were investigated for both increasing the non-metallic content of the composites for improved wear resistance and obtaining an abrupt gradient in the composite composition.

(d) Low volume-fraction composites with the finer, 5 μm-sized, additions of Al_2O_3 show tensile strengths comparable to those of matrix alloys. However, in general, the ducility of the composites decreases with increasing volume-fraction of non-metallic additions.

(e)Aluminium matrices containing high weight per cent of hard non-metals exhibit excellent friction and wear properties when tested against an AISI 52100 ball-bearing on a pin-on-disc machine. For example, composites of Alloy 2024 plus 20 wt% of 142 μm-sized Al_2O_3 particles showed a weight-loss of about 2 orders of magnitude less than that of the matrix alloy prepared and tested under identical conditions.

(f) Aluminium alloys containing SiC particles showed slightly superior wear resistance, due to their greater hardness of SiC.

(g) The wear mechanism of the matrix alloys under the test conditions was consistently adhesive in nature. On the other hand, composites with high weight per cent of non-metals showed an abrasive wear mechanism on both the disc and the steel ball-bearing.

Acknowledgment

This research was supported by the Army Materials and Mechanics Research Center, Watertown, Massachusetts, under Contract number DAAG46-76-C-0046 and was carried out at the University of Illinois, Urbana. Technical monitor of the contract was Mr. R. Gange. The 200 ton Autoforge press used in the composite forming system was donated, by the Doehler–Jarvis Division of NL Industries, Inc., to the University of Illinois at Urbana, Illanois.

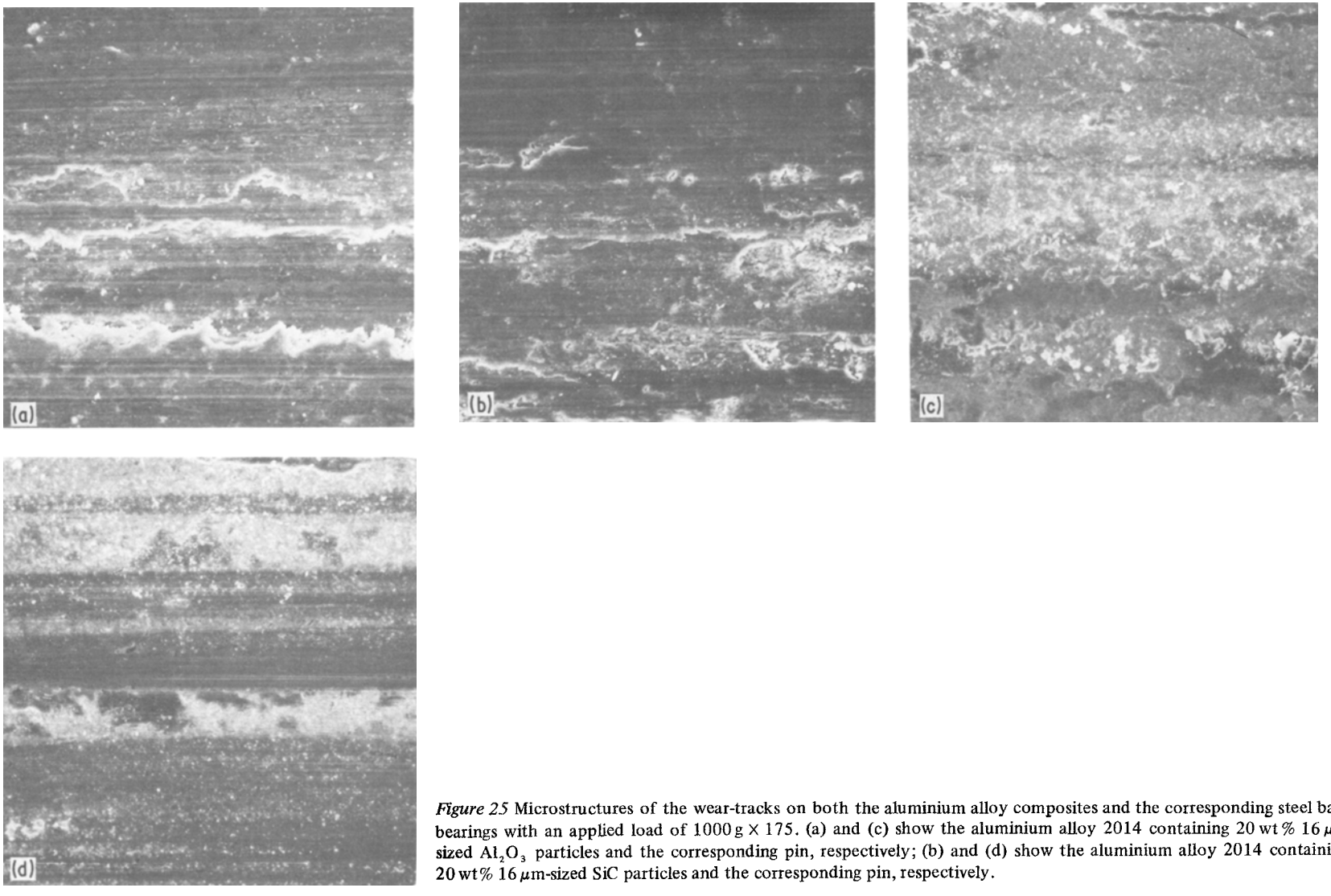

Figure 25 Microstructures of the wear-tracks on both the aluminium alloy composites and the corresponding steel ball-bearings with an applied load of 1000 g × 175. (a) and (c) show the aluminium alloy 2014 containing 20 wt % 16 μm sized Al_2O_3 particles and the corresponding pin, respectively; (b) and (d) show the aluminium alloy 2014 containing 20 wt % 16 μm-sized SiC particles and the corresponding pin, respectively.

References

1. R. MEHRABIAN, R. G. RIEK and M. C. FLEMINGS, *Met Trans.* **5** (1974) 1899.
2. A. SATO and R. MEHRABIAN, *ibid.* **7B** (1976) 443.
3. B. I. EDELSON and W. M. BALDWIN, Jr, *Trans. ASM* **55** (1962) 230.
4. C. G. LEVI, G. J. ABBASCHIAN and R. MEHRABIAN, *Met. Trans.* **9A** (1978) 697.
5. A. MUNITZ, M. METZGER and R. MEHRABIAN, *ibid.* **10A** (1979) 1491.
6. K. J. BHANSALI, in "Wear of Materials" Proceedings of the Conference on Wear of Materials (American Society of Mechanical Engineers, 1979) p. 146.
7. V. GOLOGAN and T. S. EYRE, *Wear* **28** (1974) 49.
8. R. D. ARNELL, A. P. HEROD and D. G. TEER, *ibid.* **31** (1975) 237.
9. A. V. LINEAL and H. E. HINTERMANN, in "Wear of Materials" Proceedings of the Conference on Wear of Materials (American Society of Mechanical Engineers, 1979) p. 403.
10. S. HOGMARK, O. VINGH and S. FRIDSTORM, *Wear* **31** (1975) 39.
11. D. NATH, S. K. BISWAS and P. K. ROHATGI, in "Wear of Materials" Proceedings of the Conference on Wear of Materials (American Society of Mechanical Engineers, 1979) p. 161.
12. C. BEESLAY and T. S. EYRE, *Tribology Intl.* **9** 2 (1976) 63.
13. R. SHIVANATH, P. K. SENGUPTA and T. S. EYRE, "Source Book on Wear Control Technology" (American Society for Metals, Cleveland, Ohio, 1978).
14. J. T. BURWELL and C. D. STRANGE, *J. Appl. Phys.* **23** (1953) 18.
15. C. Y. CHEN, J. A. SEKHAR, D. G. BACKMAN and R. MEHRABIAN, *Mater. Sci. Eng.* **40** (1979) 265.

Received 27 April
and accepted 15 July 1981